CALCIUM CARBONATE SATURATION HORIZONS IN THE GULF OF MEXICO

A Thesis

by

CONSTANCE SOPHIA PREVITI

Submitted to the Office of Graduate and Professional Studies of
Texas A&M University
in partial fulfillment of the requirements for the degree of

MASTER OF SCIENCE

Chair of Committee,	Shari Yvon-Lewis
Committee Members,	Kathryn E. Shamberger
	E. Brendan Roark
Head of Department,	Shari Yvon-Lewis

August 2017

Major Subject: Oceanography

ABSTRACT

The calcium carbonate saturation state is decreasing globally in the surface waters due to the increase in carbon dioxide in the atmosphere and dissolved carbon dioxide in the oceans. Recent evidence suggests that the calcium carbonate saturation horizons in the deep water of Atlantic, Pacific, and Indian Oceans are shoaling due to this influx of anthropogenic carbon to the water. The marginal seas, including the Mediterranean, Caribbean, and Gulf of Mexico, have limited inorganic carbon data to map these saturation horizons or observe the changes in depth due to anthropogenic carbon. The aragonite saturation horizons (ASH) at stations throughout the deep water of the Gulf of Mexico (GOM) were observed at an average depth of about 500m. This is much shallower than the ASH in the northwestern Atlantic (~3000m). The ASH in the GOM also gets shallower from east to west across the basin. This is due to acidified source water entering and filling the Caribbean basins and flowing into the GOM and also due to respiration occurring in the GOM.

ACKNOWLEDGEMENTS

I would like to thank my committee chair, Dr. Shari Yvon-Lewis, and my committee members, Dr. Katie Shamberger, and Dr. Brendan Roark, for their guidance and support throughout the course of this research.

Thanks also go to my friends and colleagues and the department faculty and staff for making my time at Texas A&M University a great experience.

Finally, thanks to my family and friends for love, patience, and clarity in this endeavor.

CONTRIBUTORS AND FUNDING SOURCES

Contributors

This work was supervised by a thesis committee consisting of Dr. Shari Yvon-Lewis [advisor], Dr. Kathryn Shamberger of the Department of Oceanography, and Dr. Brendan Roark of the Department of Geography.

The data for GISR 01 and GISR 06 were analyzed by Jordan Young. The data from GOMECC1 and GOMECC2 were published in 2013 and 2015 respectively for public use. The data from WOCE A22 and the repeat CLIVAR section of A22 were obtained from https://doi.org/10.21976/C6RP4Z.

Special thanks to discussions provided by Dr. Piers Chapman, Dr. Ann Jochens, Dr. Alex Orsi, and Dr. Steve DiMarco. All other work conducted for the thesis was completed by the student independently.

Funding Sources

Graduate study was supported by a Teaching Assistant fellowship from Texas A&M University. This work was made possible in part by NSF S-STEM scholarship under Award Number 1355807. This work was also supported by the Gulf of Mexico Integrated Spill Response Consortium (GISR) under the Gulf of Mexico Research Initiative.

Its contents are solely the responsibility of the authors and do not necessarily represent the official views of the GOMRI and GISR.

TABLE OF CONTENTS

Page

LIST OF FIGURES

Page

1. INTRODUCTION

Throughout the world, the ocean provides resources including food, tourism, and temperature regulation to the global climate. The global oceans are, however, in danger of devastating changes to the biological and chemical characteristics as a result of human activities. With a large increase in human activity and the increase in use of fossil fuels, there have been changes in the ocean environments that biology cannot necessarily keep up with in terms of adaptation. This includes sea level rise, temperature increases, and ocean acidification.

Ocean acidification is the process of decreasing the pH of seawater due to the uptake and dissolution of excess anthropogenic carbon dioxide (CO_2) being added to the atmosphere due to burning fossil fuels, land use changes, and other human activities [Millero, 2007]. It affects chemical, geological, and biological aspects of the oceans by impacting the dissolution rates of calcium carbonate. The reactions of acidification are:

$$CO_2 + H_2O \leftrightarrow H_2CO_3^* \quad (1)$$

$$H_2CO_3 \leftrightarrow H^+ + HCO_3^- \quad (2)$$

$$HCO_3^- \leftrightarrow H^+ + CO_3^{2-} \quad (3)$$

$$Ca^{2+} + CO_3^{2-} \leftrightarrow CaCO_3 \quad (4)$$

The dissolution of CO_2 into water (H_2O) produces $H_2CO_3^*$ which is equal to the sum of aqueous carbon dioxide ($CO_{2(aq)}$) and carbonic acid (H_2CO_3) (equation1). H_2CO_3 immediately dissociates in seawater (equation 2) where the product is a proton (H^+) and bicarbonate (HCO_3^-) [Millero, 2007]. Equation 3 shows the dissociation of HCO_3^- into another proton and a carbonate ion (CO_3^{2-}). This reaction is generally more favored to go

to the left in seawater during ocean acidification due to the increased concentration of protons. This reaction decreases the concentration of carbonate ions present in the water as the amount of protons increases. Equation 4 represents the dissolution and production of calcium carbonate ($CaCO_3$) where Ca^{2+} is the calcium ion [Millero, 2007].

Acidification affects the organisms that form shells and skeletons out of $CaCO_3$ in two main ways: (1) $CaCO_3$ will dissolve when the pH is lowered and (2) CO_3^{2-} will be unavailable for new shell building. This includes the planktonic species that define the base of the food web in the ocean such as coccolithophores. Because the concentration of CO_3^{2-} decreases due to acidification, the saturation state of $CaCO_3$ also decreases leading to faster dissolution rates and slower calcification rates of $CaCO_3$. The saturation state (Ω) is calculated from:

$$\Omega = [Ca^{2+}]\,[CO_3^{2-}]/K_{sp} \qquad (5)$$

where $[Ca^{2+}]$ is the concentration in mol/L of the calcium ion, $[CO_3^{2-}]$ is the concentration of carbonate ion mol/L, and the K_{sp} is the solubility product (mol^2/L^2) of the reaction in equation 4 (Manno et al., 2007). Decreasing the saturation state leads to faster dissolution rates and slower calcification rates in the surface waters [Barrett et al., 2014]. Aragonite and calcite are the two main forms of calcium carbonate in the ocean. Due to differences in their respective mineral structures, the aragonite form is more soluble than calcite in seawater [Byrne et al., 1984; Manno et al. 2007]. When Ω is greater than 1, the water is supersaturated with respect to $CaCO_3$, so organisms have more carbonate ions available to build structures [Honjo and Erez, 1978]. When Ω is less than 1, the water is undersaturated with respect to $CaCO_3$ meaning that there is less

$[CO_3^{-2}]$ available in the water and $CaCO_3$ dissolution is thermodynamically favored. Because the saturation states of both aragonite (Ω_a) and calcite (Ω_c) decrease with depth in the water column, there is a transition from supersaturated to undersaturated water where Ω is equal to 1. This transition is defined as the saturation horizon and exists at different depths for both aragonite and calcite [Honjo and Erez, 1978].

The solubility of $CaCO_3$ increases with decreasing temperature and increasing pressure and acidity, leading to slower calcification rates and enhanced dissolution rates with depth. This increase in the dissolution rates also changes sedimentation rates in the deep ocean and can affect the sequestration of carbon into the sediments [Barret et al., 2014]. Due to the solubility characteristics of $CaCO_3$, the progression of ocean acidification, and the economic importance of calcifying organisms (oyster farms, coral reefs, etc.), monitoring the changes of aragonite and calcite saturation state in the water column is important [Wang et al., 2013].

Dissolved inorganic carbon (DIC), which is the sum of the concentrations of all inorganic carbon species (equation 6), along with Total Alkalinity (TA), the buffering capacity of seawater (equation 7), govern the saturation state of $CaCO_3$.

$$DIC = [CO_2] + [H_2CO_3] + [HCO_3^-] + [CO_3^{2-}] \quad (6)$$

$$TA = [HCO_3^-] + 2[CO_3^{2-}] + [B(OH)_4^-] + [OH^-] + \ldots - [H^+] \quad (7)$$

The sum of the species in Equation 7 buffer against acidification where $[B(OH)_4^-]$ is the concentration of borate and $[H^+]$ is the concentration of protons or the amount of acid present in seawater. Concentrations of the nutrients, including phosphate and nitrate ions, are also taken into account as the ellipses term but are such a small part of the

overall buffering capacity that they are often negligible. The negatively charged ions effectively balance out the positively charged acid to prevent large changes in pH through the reactions defined in equations 3 and 4 [Manno et al., 2007; Barret et al., 2014].

On average, DIC increases with depth [Goyet et. al., 2000]. This is due to photosynthesis at the surface taking up CO_2 and respiration below the euphotic zone introducing CO_2 at depth. TA is dependent on the sources of carbonate and other buffering species in the ocean [Carter et al., 2014], but also on the amount of dissolution of $CaCO_3$. When $CaCO_3$ shells or other structures dissolve, the carbonate ion is used in the buffering system [Manno et al., 2007]. Some river systems, including the Mississippi River system in the northern Gulf of Mexico, bring high amounts of alkaline waters to the ocean allowing the Gulf of Mexico to have a high buffering capacity against ocean acidification in the surface waters and into intermediate waters [Wang et. al., 2013]. Because DIC increases with depth and the solubility of $CaCO_3$ increases with increasing pressure and decreasing temperature, the overall saturation states of both aragonite and calcite decrease with depth [Thunell, 1982]. The dependence of the saturation horizons on DIC and TA leads to the global saturation horizons varying by ocean and region as DIC and TA vary by ocean and region.

1.1 GLOBAL SATURATION HORIZONS

Globally, $CaCO_3$ saturation horizons are separated into two separate horizons that are characterized by the two main forms of calcium carbonate: aragonite and calcite. The aragonite saturation horizon (AHS) is shallower than the calcite saturation

horizon (CHS) because aragonite is more soluble than calcite in seawater. This solubility parameter defines the types of reef structures found in the deep waters throughout the global oceans. Most deep-sea scleractinian corals form aragonite structures and can therefore be found in the parts of the Atlantic where the aragonite saturation horizon is deep and are often rare in the deep waters of the Pacific [Guinotte et al., 2006]. With the addition of anthropogenic carbon, the saturation horizons are getting shallower and will continue to get shallower as the ocean continues to uptake anthropogenic carbon dioxide [Feely et al., 2004; Sabine et al., 2004; Sarma et al., 2002]. This phenomenon could cause problems for the deep-sea corals and the diverse ecosystems they support.

In the Pacific, the aragonite and calcite saturation horizons are relatively shallow. In the North Pacific, the depth of the aragonite saturation horizon ranges from 120m to 580m and shoals from west to east [Feely et al., 2002]. The calcite saturation horizon ranges from 250 to 2750m in the same region and is shallower in the eastern Pacific [Feely et al., 2002]. The eastern Pacific has large regions of upwelling along the western coasts of North and South America. These regions of upwelling bring acidified waters up from intermediate depths. The deep water in the North Pacific originates in areas of deep water formation in the North Atlantic and Southern Ocean. North Atlantic Deep Water (NADW) mass moves away from it source in the North Atlantic it circulates down towards the Southern Ocean and into the Indian and Pacific Oceans. In the northern Pacific, the NADW is much more acidic than it was at its source because of the respiration that occurs along the circulation pathway from the northern Atlantic Ocean to the northern Pacific Ocean. The Southern Ocean takes up approximately 30-40% of

global anthropogenic carbon dioxide [Sabine et al., 2004]. Although the Southern Ocean uptakes a large percentage of anthropogenic carbon, the storage rates are low. This is in part due to the production of Antarctic Bottom Water (AABW) that travels northward out of the Southern Ocean into the Indian, Atlantic, and Pacific Oceans. Because AABW is formed in a region that takes up large amounts of CO_2, the water is therefore more acidic than other water masses. As AABW travels to the Pacific, the already acidic waters are exposed to respiration at depth. The deep water in the Pacific is not ventilated, so the waters become increasingly acidic as the bottom water travels north and east across the basin. This leads to shallow calcium carbonate saturation horizons in the Pacific especially in the North Pacific.

In the Indian Ocean, the aragonite saturation horizon exists between 240m and 1200m [Sarma et. al., 2002] and gets shallower northward in a matter similar to the Pacific. The calcite saturation horizon stays between 3200m and 3400m throughout the southern Indian Ocean [Bostock et al., 2013]. Similar to the Pacific, the CHS is also shallower in the northern Indian Ocean versus the southern Indian Ocean.

The aragonite saturation horizon is between 750 and 2750m in throughout the Atlantic including shallow enclosed horizons in the northern hemisphere due to Mediterranean Overflow Water (MOW) [Friis et al., 2007; Chung et al., 2003]. In the northern Atlantic, the AHS exists around 3000m in both the western and eastern sides of the basin [Chung et al., 2003]. The calcite saturation horizon is between 3000m and 5000m in both the North and South Atlantic [Chung et al., 2003]. The South Atlantic aragonite saturation horizon ranges from 1000 to 3000m [Chung et al., 2003]. There is significant shoaling of

the aragonite saturation horizon along the southwestern coast of Africa, as a result of upwelling. There is not a significant signature of the calcite saturation horizon upwelling in this same region because the calcite saturation horizon is not shallow enough for it to be upwelled. The horizon gets shallower in the southern Atlantic. There is also a shallower region in the water column of the northeastern Atlantic as a result of the presence of Mediterranean Intermediate Water (MIW) with a shallow horizon near the equator [Chung et al., 2004].

For all aragonite and calcite saturation horizons in all oceans, there is observed shoaling due to uptake of anthropogenic CO_2 [Feely et al. 2004]. In the Pacific, the horizons have shoaled approximately 1-2m/yr since the industrial revolution with faster rates occurring within the last few decades [Feely et al, 2012]. Shoaling of the horizon, specifically due to anthropogenic carbon, was also observed in the Indian Ocean at a rate of 0.2-2.2m/yr between 1974 and 1994 [Sarma et al., 2002]. Although the Atlantic saturation horizons are relatively deep, there was also observed shoaling in a few places in the south Atlantic and the western North Atlantic at a rate of 0.5-0.75m/yr since the industrial revolution [Chung et al., 2003].

The marginal seas of the global oceans, including the Mediterranean and the Gulf of Mexico, have not yet been mapped in terms of calcium carbonate saturation horizons. This is due to a lack of inorganic carbon data collected at depth for these areas. These regions have important coral systems and other carbonate utilizing marine organisms present that provide biodiversity, tourism opportunities, and fishing grounds. These ecosystems will also be impacted by the global change in saturation horizon depths.

1.2 GULF OF MEXICO

The Gulf of Mexico (GOM) is unique in both its physical properties and its economic importance. For both the United States and Mexico, the gulf provides many resources including fish, tourism, and petroleum. The GOM is a relatively shallow, semi-enclosed basin with an average water depth of 1615 m and a maximum depth of

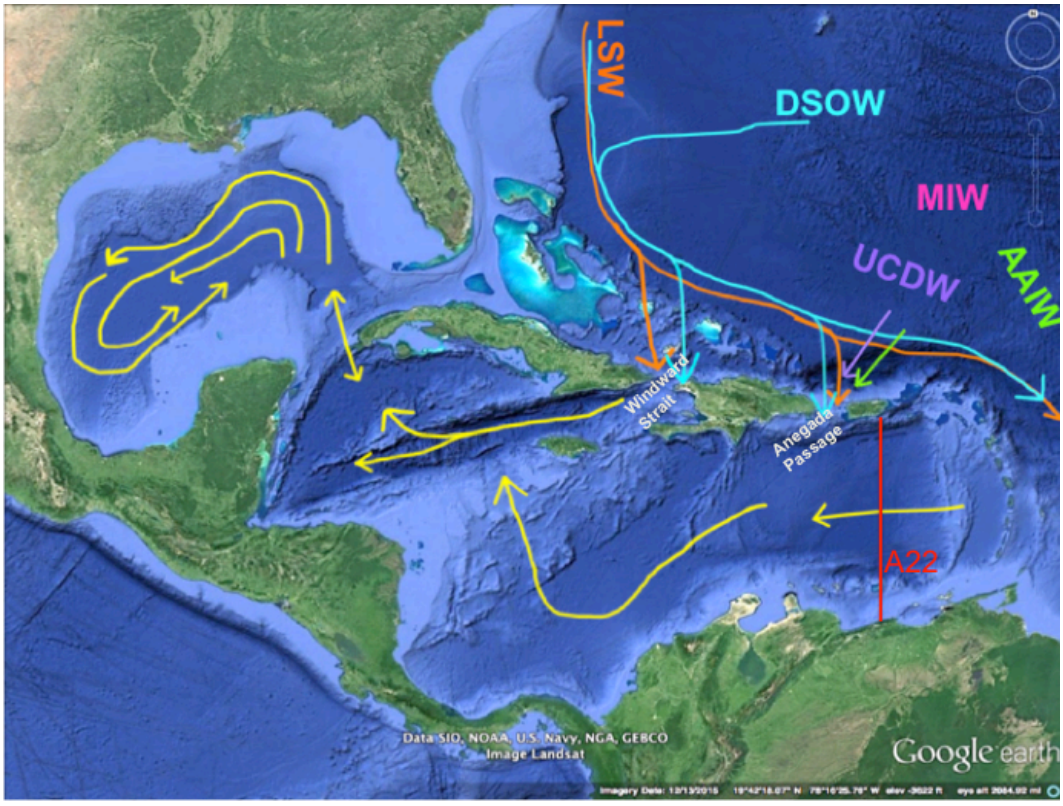

Figure 1: Map of Caribbean Sea and the Gulf of Mexico showing where deep water enters the Caribbean from the Atlantic Ocean and the approximate flow of deep water through the Caribbean and around the Gulf of Mexico. Deep and intermediate water masses are indicated including deep western boundary current (DWBC) containing both Labrador Sea Water (LSW) and Denmark Strait Overflow water (DSOW), Antarctic Intermediate Water (AAIW), and Mediterranean Intermediate Water (MIW). These water masses exist between 5000-1000m [Talley et al., 2011]. Size of the arrows does not indicate flow rate. [Jochens and DiMarco, 2008; Gordon, 1967; Osbourne et al., 2014; Sheng and Tang, 2003; Nof, 2000; Joyce et al., 1999; Sturges, 1970; Rivas et al., 2005]

4384 m. It has a wide flat continental shelf that is widest on the eastern side of the gulf off of the Yucatan Peninsula and western Florida. It also has an extensive barrier island system mainly off the coast of Texas.

The main source of surface seawater enters through the Yucatan Strait and forms the Loop Current in the surface water. The surface water exits through the Florida Strait becoming the Florida Current and eventually the Gulf Stream. Warm core and some cold core eddies often break off of the loop current and travel into the northern and western GOM [Maul and Vukovich, 2003]. The Loop Current is the main surface current that occurs at the surface in the GOM other than the freshwater influxes. There are 20 river systems that feed the gulf. In the northern gulf, the main major river system is the Mississippi river system [Nipper et al., 2008]. This water is characterized by a TA between 1600-2500 μmol/kg due to geologic traits of the river pathway [Keul et al., 2010]. This results in a 3.9-9.7 aragonite saturation state in the river and river plume [Keul et al., 2010; Wang et al., 2013]. Both TA and $CaCO_3$ saturation state from the Mississippi can be traced in the Mississippi river plume and throughout the surface waters of the northern Gulf of Mexico [Cai, 2003]. Entrainment of the high TA surface water is observed due to the Loop Current and formation of eddies [Wang et al., 2013]. Deep water circulation in the Gulf of Mexico is governed by inflow of water from the Caribbean (Figure 1). The deep water enters the Caribbean from the Atlantic in two places: over the sill (1600-2000m) at the Anegada-Jungfern Passage and over the sill (1600m) at the Windward Strait [Stalcup et al., 1975; Fatantoni et al., 1997; Sturges, 1970; Rivas et al., 2005]. Water moving over the Anegada-Jungfern sill enters the

Venezuela basin from the southeast, while water moving over the Windward Strait enters the Cayman basin from the north. The basins are separated by the Jamaican rise. The deep water enters and exits the GOM through the Yucatan Strait at a sill depth of 2040 m. The Florida Strait is too shallow to allow for deep water passage with a sill depth of 740 m, so the outflow of deep water goes back through the same strait [Rivas et al., 2005].

Because the only deep water that can enter the Caribbean and the Gulf of Mexico comes from the Atlantic Ocean, the possible deep water masses in the basins are Antarctic Intermediate Water (AAIW) that is characterized by low oxygen and North Atlantic Deep Water (NADW) that has oxygen levels between 240-275 μM/kg [Talley et al., 2011]. In the GOM, the AAIW sits between 600 and 900m just above the NADW at around 1000 m [Rivas et al., 2005]. The deep water flows in the cyclonic direction inside the GOM basin below 1500m (Figure 1) [DeHaan and Sturges, 2005; Jochens and DiMarco, 2008]. Rivas et al. [2005] estimates the residence time of the GOM deep water to be only about 250 years based on increased oxygen values in the deep water of the Yucatan Strait. However, this study did not distinguish between inflowing water from the Caribbean or outflowing water from the Gulf of Mexico, which may bias their results towards a residence time that is too short. Nonetheless, this is the best estimate of the residence time of GOM deep water to date.

In the GOM, the Oxygen Minimum Zone (OMZ) occurs between 400 and 600m. Both respiration of falling organic matter and hydrocarbon dissolved organic carbon

affect the dissolved oxygen concentration [Pohlman et al., 2010]. Respiration also introduces carbon dioxide in the water column through the following equation

$$C_6H_{12}O_6 + 6O_2 \rightarrow 6CO_2 + 6H_2O \quad (8)$$

where $C_6H_{12}O_6$ represents glucose and O_2 represents oxygen gas. Although glucose is represented in the equation above as the carbon source, the consumption of dissolved organic carbon and other organic matter by microbes in the water column is not limited to glucose. Respiration occurs in the water column below the euphotic zone due to remineralization of organic matter and is often indicated by a decrease in dissolved oxygen concentration within the water column called the OMZ [Paulmier et al., 2011]. Generally, oxygen is high at the surface due to photosynthesis and air sea interactions. Below the surface, oxygen concentration decreases slowly below the euphotic zone starting around 50m and continuing to decrease until the OMZ [Paulmier et al., 2011]. After the Deepwater Horizon Oil Spill in 2010, there was a significant oxygen drawdown that occurred within the hydrocarbon plume emitted from the wellhead that resulted from microbial respiration of hydrocarbons [Hazen et al., 2010; Du and Kessler, 2012]. With the consumption of oxygen during respiration, there is expected to be an increase in CO_2, especially when there is labile methane or other labile hydrocarbons [Pohlman et al., 2010].

Another feature of the Gulf of Mexico is the large number of hydrocarbon seeps that exist across the continental shelf, the continental slope, and the deep sea floor. There are approximately 20,000 known seeps that are located mainly in the central northern and western slopes and along the seafloor [Joye et al., 2016]. Most seeps were identified

through seismic bottom water analysis, and both methane and oil are emitted into the water column. They are often used in the oil industry as indicators of larger oil reservoirs for drilling. The seeps emit approximately 120,000 barrels of hydrocarbons into the water column of the GOM every year greatly affecting the water chemistry locally around the seeps and also throughout the water column [MacDonald et al., 1998; MacDonald et al., 2005]. The methane emissions also reach the atmosphere and the GOM acts as a significant source of methane to the atmosphere [Solomon et al., 2009]. The seeps also dictate the biological ecosystems along the central slope [Cordes et al., 2009]. These ecosystems include corals and reef systems, and they rely on the influx of hydrocarbons [Georgian et al., 2015; Guinotte et al., 2006; Lunden et al., 2013]. Authigenic carbonates are also formed around the seeps as a result of the hydrocarbon influx [Mansour, 2013]. These seeps allow for many different communities to thrive in these deep sea areas. In the sediment pore waters, there is anaerobic respiration of these hydrocarbons increasing alkalinity and creating authigenic precipitates of carbonates [Naehr et al., 2009]. This is a way corals and other carbonate-utilizing organisms can thrive despite the acidic conditions of the water column at depth. Because seeps dictate so many different characteristics of the Gulf of Mexico, they are an important part of the analysis of the aragonite saturation horizons.

There has been little data detailing the inorganic carbon system in the deep Gulf of Mexico. By looking at DIC and TA depth profiles, the saturation horizons can be examined in the GOM. In 2013, Wang et. al examined the coastal carbon system in the GOM and along the east coast of the United States using data collected during Gulf of

Mexico East Coast Carbon 1 cruise (GOMECC 1). Wanninkhof et al. 2015 presented GOMECC 2 cruise data and compared it to GOMECC 1. Only 4 stations from each cruise went into deep water in the GOM, and all of these stations were located off of the western shelf of Florida. Although Georgian et al. published carbonate chemistry data in the deep water of the northern GOM, they did not find an ASH in these data. These studies are the only published deep water inorganic carbon data available for the Gulf of Mexico at present time.

2. METHODS

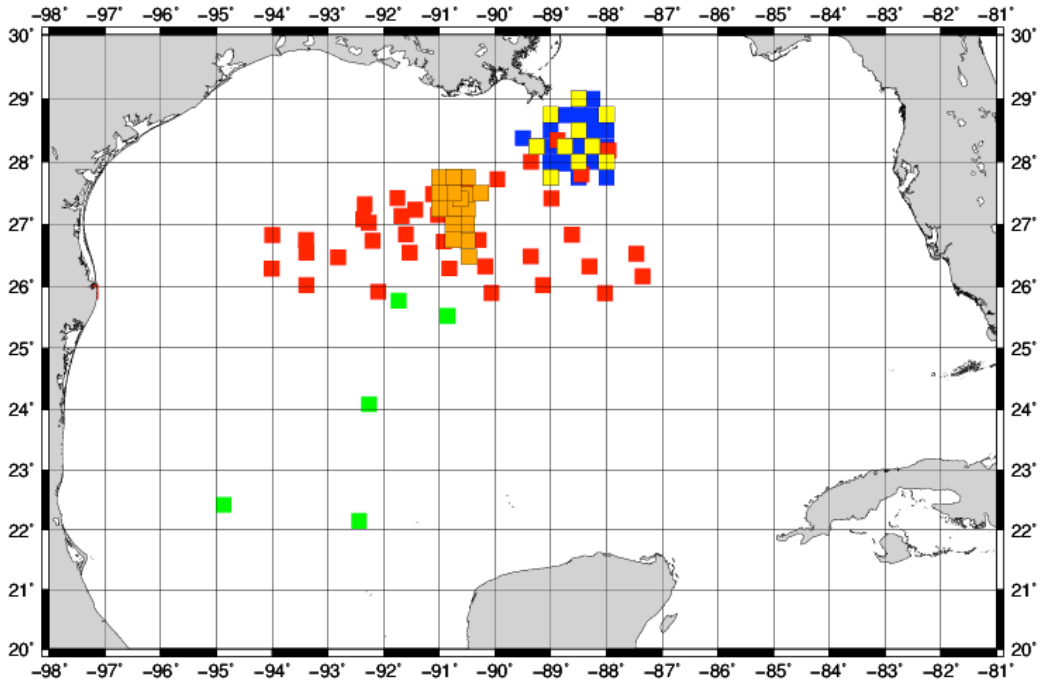

Figure 2: Map of the Gulf of Mexico depicting sampling stations for each of the GISR cruises: G01 (blue), G03 (red), G05 (green), G06 (yellow), and G09 (orange).

Data were collected from 5 separate cruises funded by the Gulf of Mexico Research Initiative (GoMRI) through the Gulf of Mexico Integrated Spill Response (GISR) consortium (Figure 2): G01 (Chief Scientist: Steven DiMarco), G03 (Chief Scientist: James Ledwell), G05 (Chief Scientist: James Ledwell), G06 (Chief Scientist: Steven DiMarco), and G09 (Chief Scientist: Steven DiMarco). These cruises covered the central and northern GOM with some stations in Mexican waters. G01 occurred from 5 July 2012 to 11 July 2012 and was confined to the area directly off the Mississippi River delta. G03 occurred from 28 November 2012 to 20 December 2012 in the northern and in deep water of the GOM (25.8934°N to 28.3486°N and -97.2617° to -87.3498°). G05

occurred from 29 July 2013 to 27 August 2013 and was located mainly in the deep water of the GOM with some stations in the Mexican deep waters (29.25467°N to 21.3622°N and 97.0643°W to 45.39013°W). G06 occurred from 25 June 2014 to 30 June 2014 in the northern GOM close to the Mississippi delta (27.75084°N to 29.00026°N and 89.24964°W to 87.99966°W). G09 occurred from 13 April 2015 to 19 April 2015 in the northern GOM and was located around GC600 (a known methane seep site) (26.4822°N to 28.2475°N and 89.7490°W to 87.0002°W) (Figure 2).

During each cruise, water samples for DIC analysis were collected in 350mL and 500mL bottles from rosettes from each CTD cast and poisoned with 100µL (for 350mL bottles) and 200µL (for 500mL bottles) of HgCl in each sample before sealing All samples were kept in a cold room at 4°C until analysis. These DIC samples were analyzed starting in May of 2015 and ending in December of 2015. The DIC samples were analyzed using a Versatile Instrument for the Determination of Total inorganic carbon and titration Alkalinity (VInDTa) system. Each water sample was titrated with an excess amount of 6.4M H_3PO_4 (12.5 mL concentrated H_3PO_4 and 37.5 mL low organic carbon H_2O made daily) to convert all dissolved inorganic carbon to CO_2 gas. The amount of CO_2 gas per sample was analyzed in a coulometer and reported as counts [Dickson et al., 2007]. All samples were calibrated against certified reference material (CRM) samples made by Dickson at the Scripps Institute of Oceanography. The counts were converted to DIC concentration in µmol/mL through the following calculation:

$$DIC = [((C_s)-(bl)*(t_r))/(Cal)]*[1/(v*1.025)] \quad (9)$$

Where C_s is the sample counts, bl is the blank value for the analysis day, t_r is the run time of the sample, Cal is the CRM calibration factor, and v is the titrated sample volume. The CRM calibration factor was calculated for each of the two separate runs of the same sample of certified reference material using the following equation:

$$Cal = [((CRM_a\text{-}C_{CRM})\text{-}(bl)(t_{CRM}))/(CRM_t)(v)(1.025))]*10^6 \quad (10)$$

Where CRM_a is the measured CRM concentration, C_{CRM} is the counts for the CRM sample, t_{CRM} is the run time of the CRM sample, and CRM_t is the theoretical CRM concentration. The two calibration factors were averaged for use in calculating DIC for the samples.

During the analysis of both G01 and G03, the intensity of the lamp in the coulometer was increased. This caused some DIC data points to be significantly lower than the average measurements for DIC. These data were removed, and all reported data do not include these values. The percent error for DIC was calculated per analysis day based on differences between multiple CRM run values. The percent error was used to calculate the precision for the DIC values. The average precision of the DIC measurements for the GISR cruises was +/- 6.07.

After each sample was analyzed for DIC, it was then analyzed for TA using an open-cell auto-titrating method. Each day, the alkalinity system was calibrated with TRIS and AMP buffers and two separate runs of a CRM sample according to methods

defined by Dickson et al. (2007). For every bottled sample, 50mL of the water sample was placed into a temperature controlled jacketed beaker at 20°C and was titrated using 0.024M HCl/NaCl/low organic carbon water titrant. The files created from the alkalinity titration software were used to calculate the total alkalinity of the sample in μmol/mL. Percent error for TA was calculated per analysis day based on differences between multiple CRM run values. The percent error was used to calculate the precision for TA values as mentioned above for the DIC values. The average precision for TA was +/- 10.6. Although both precision values are high, the TA measurements are less precise than in the DIC measurements suggesting that the alkalinity instrumentation may contain some issues. Using both the values for DIC and alkalinity, CO2SYS was used to calculate pH and saturation states of calcite and aragonite. [Pierrot et al., 2006] The error range for calculated parameters were calculated through a series of steps. First, the daily DIC precision values were added to the DIC values to "maximum DIc" values, and the daily TA precision values were subtracted from the TA values to get "minimum TA" values. Next the "maximum DIC" values along with the "minimum TA" values were inputed into CO2sys to calculate saturation states, pH, pCO_2, and CO_3^{2-}. These new parameter values represented the parameters that included the maximum possible error range. The actual error range shown as error bars in the following figures was calculated by subtracting he "error parameters" from each actual parameter value (saturation states, pH, pCO_2, and CO_3^{2-}) to find the maximum error value for the error range, the error parameters were added to the actual parameters. Because the error could not be calculated due to loss of data files for cruises G01 and G06, data from these cruises was

not used to calculate error in the CO2sys parameters and could not be used to show error in the following figures.

The aragonite saturation horizon was estimated for each station for every cruise by using the depth of the shallowest bottle that was undersaturated if subsequent deeper bottles were also undersaturated. The calcite saturation horizon is not reported because it was not observed in the water column (no samples were undersaturated with respect to calcite).

3. RESULTS

The salinity normalized total inorganic carbon (DIC) is relatively low at the surface and increases rapidly down to approximately 600m where it slowly decreases until around 1500m (Figure 3). There is a slight relative minimum at 1500m for stations in cruises G05, G06, and G09 (Figure 4). In G03 and G01, the slight decrease and relative minimum is less prominent in the profiles (Figure 4). After 1500m, all DIC profiles are constant throughout the deep water column until the sediment. The increase in DIC below the surface to 600m suggests the carbon dioxide is being consumed

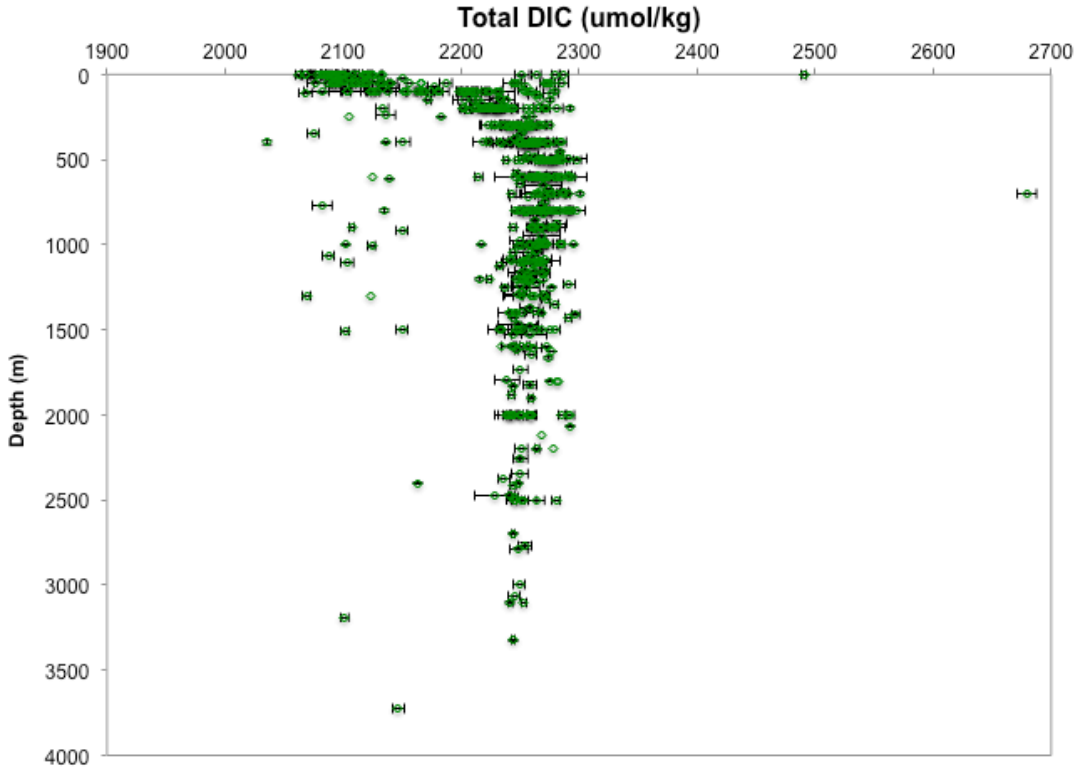

Figure 3: The total dissolved inorganic carbon (DIC) in the Gulf of Mexico plotted vs. depth at each station from every GISR cruise. Black error bars are shown for cruises G03, G05, and G09. Error bars represent the daily precision values.

through photosynthesis at the surface and produced through remineralization and respiration below the euphotic zone.

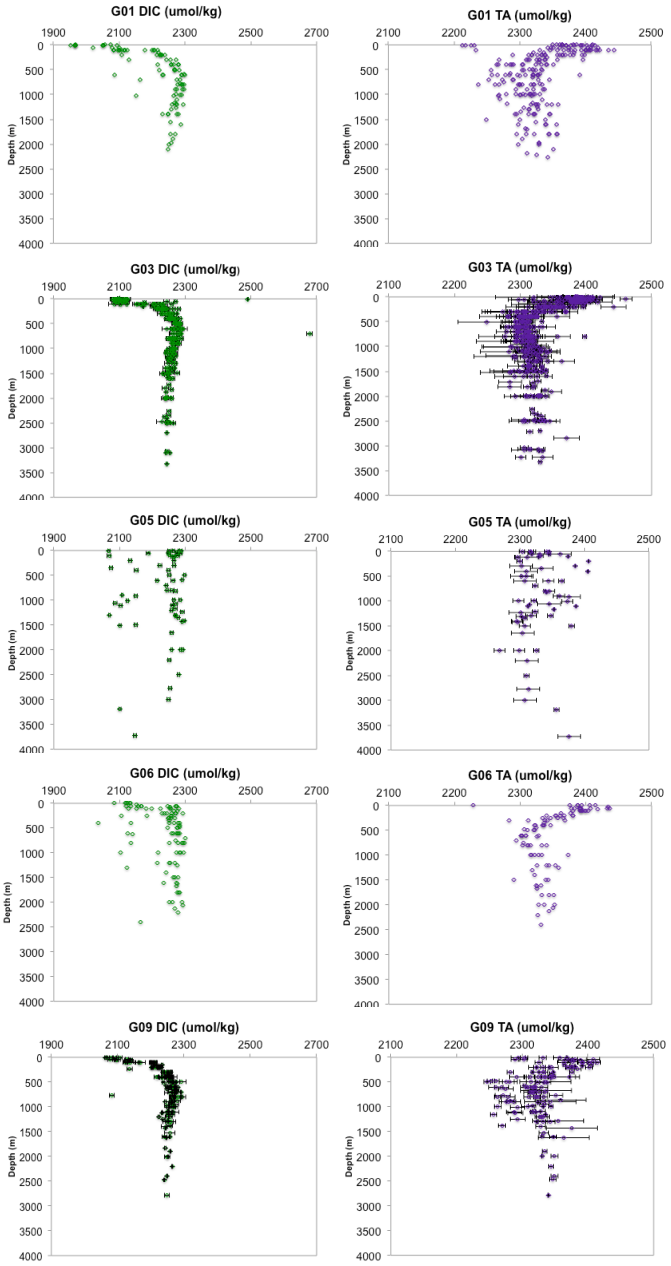

Figure 4: DIC and TA for each GISR cruise. From top row down: G01 DIC vs depth (left) and G01 TA (right), G03 DIC (left) and G03 TA (right) including error bars in black, G05 DIC (left) and G05 TA (right) including error bars in black, G06 DIC (left) and G06 TA (right), and G09 DIC (left) and G09 TA (right) including error bars in black on the bottom row. Both DIC and TA are reported in umol/kg.

Salinity normalized total alkalinity (TA) remains consistent throughout the water column with an average of 2302 umol/kg (Figure 5). However, there is a slight decrease in TA just below the surface to about 250m that is observed in all stations. G05 has the slightest decrease below the surface while G06 has the largest decrease. Below this depth, the TA profiles increase back to surface level concentration until around 700m and then continues to remain constant with increasing depth. Even though alkalinity is consistent below 1500m (Figure 5), the carbonate ion concentration, $[CO_3^{2-}]$, increases slightly below the minimum $[CO_3^{2-}]$ at 600m (Figure 6). The TA profiles from G09 show values in two almost distinct profiles (Figure 5).

As is typical for the calcium carbonate saturation in the water column, aragonite is supersaturated in the surface waters of the GOM (Figure 7). The aragonite saturation state rapidly decreases in the water column until around 500m following the increase in DIC throughout the water column. Once the aragonite saturation horizon is observed around 500m, the rate of change in aragonite saturation state stabilizes and slowly decreases throughout the rest of the water column. The ASH appears slightly shallower than the maximum DIC depth at around 600m. The calcite saturation horizon was not observed in any of the samples because the entire water column was supersaturated with respect to calcite (Figure 7). The absence of the calcite saturation horizon was also observed in the GOMECC cruise data.

Because $[CO_3^{2-}]$, pH (total scale), and the partial pressure of carbon dioxide (pCO_2), (Figure 6), were all calculated using CO2sys with TA and DIC, they should all be reliant on the patterns laid out by both the DIC profiles and the TA profiles. pH

shows a decrease from the surface value of 8.2 to the minimum around 600m (Figure 8). This pattern is consistent with the DIC patterns (Figure 3). The pH does increase below 1000m, suggesting a buffer from alkalinity. The calculated pCO_2 shows a maximum around 600m, also consistent with the maximum of DIC around 600m, and a decrease from the maximum down to 1600m and remains consistent at around 700 mmol/kg below 1600m.

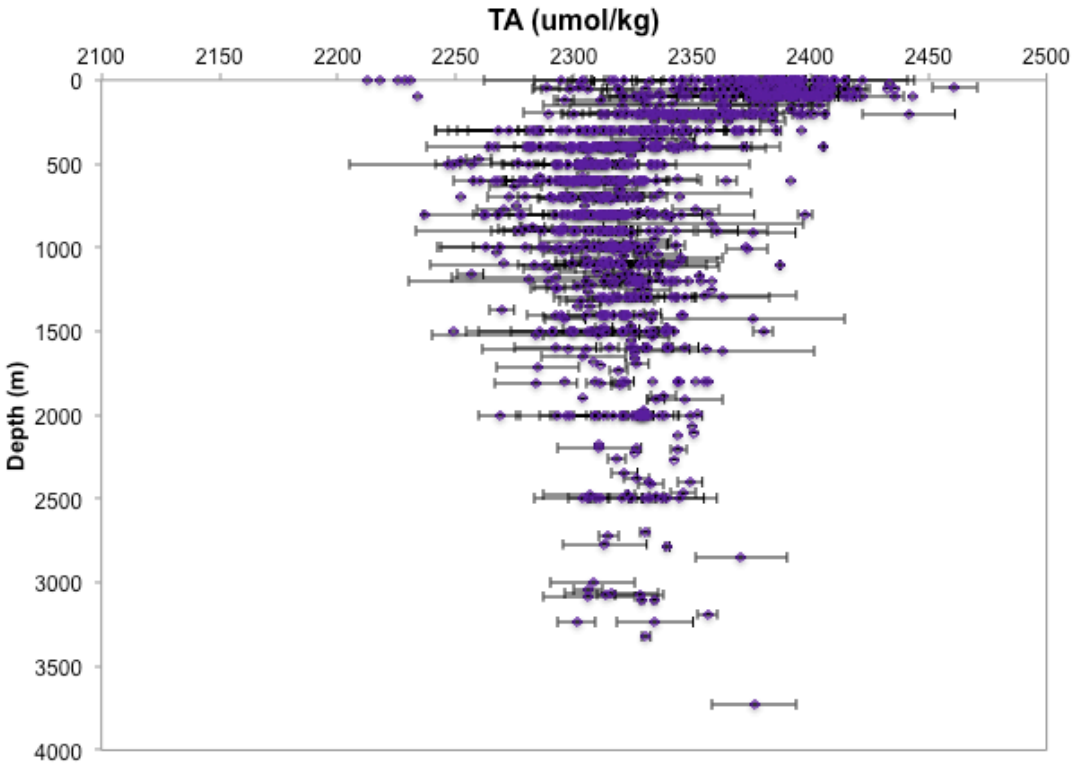

Figure 5: Compilation of salinity normalized total alkalinity (TA) values from all GISR stations. Black error bars are shown for cruises G03, G05, and G09. The error range values were calculated with CO2sys using the maximum possible DIC values along with the minimum possible TA values to find the minimum and maximum saturation state values for each bottle value.

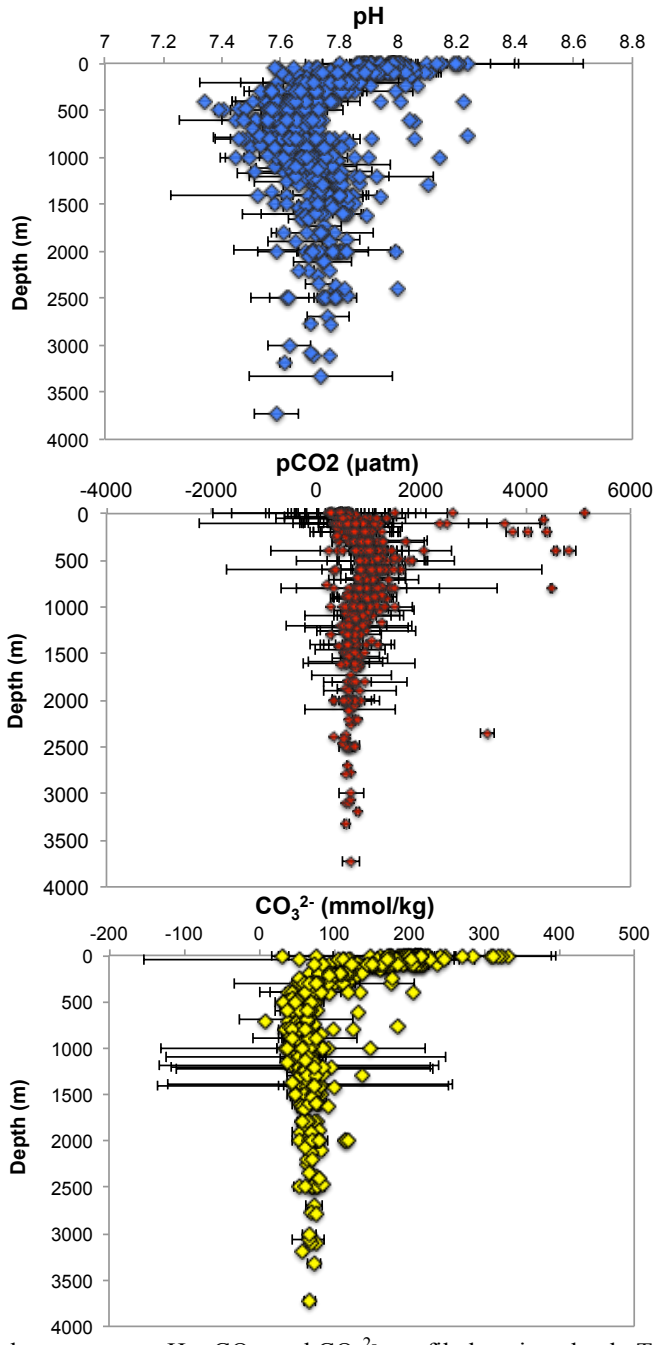

Figure 6: Calculated paramaters, pH, pCO_2, and CO_3^{2-}, profiled against depth. Top graph shows compilation of calculated pH on the total scale vs. depth in meters at all GISR stations (blue) with black error bars for cruises G03, G05, and G09. The middle graph shows the compilation of calculated pCO_2 in µatm vs. depth in meters at all GISR stations (red) with black error bars for cruises G03, G05, and G09. The bottom graph shows the compilation of carbonate ion concentration in mmol/kg vs. depth in meters at all GISR stations (yellow) with black error bars for cruises G03, G05, and G09. The error range values were calculated with CO2sys using the maximum possible DIC values along with the minimum possible TA values to find the minimum and maximum saturation state values for each bottle value.

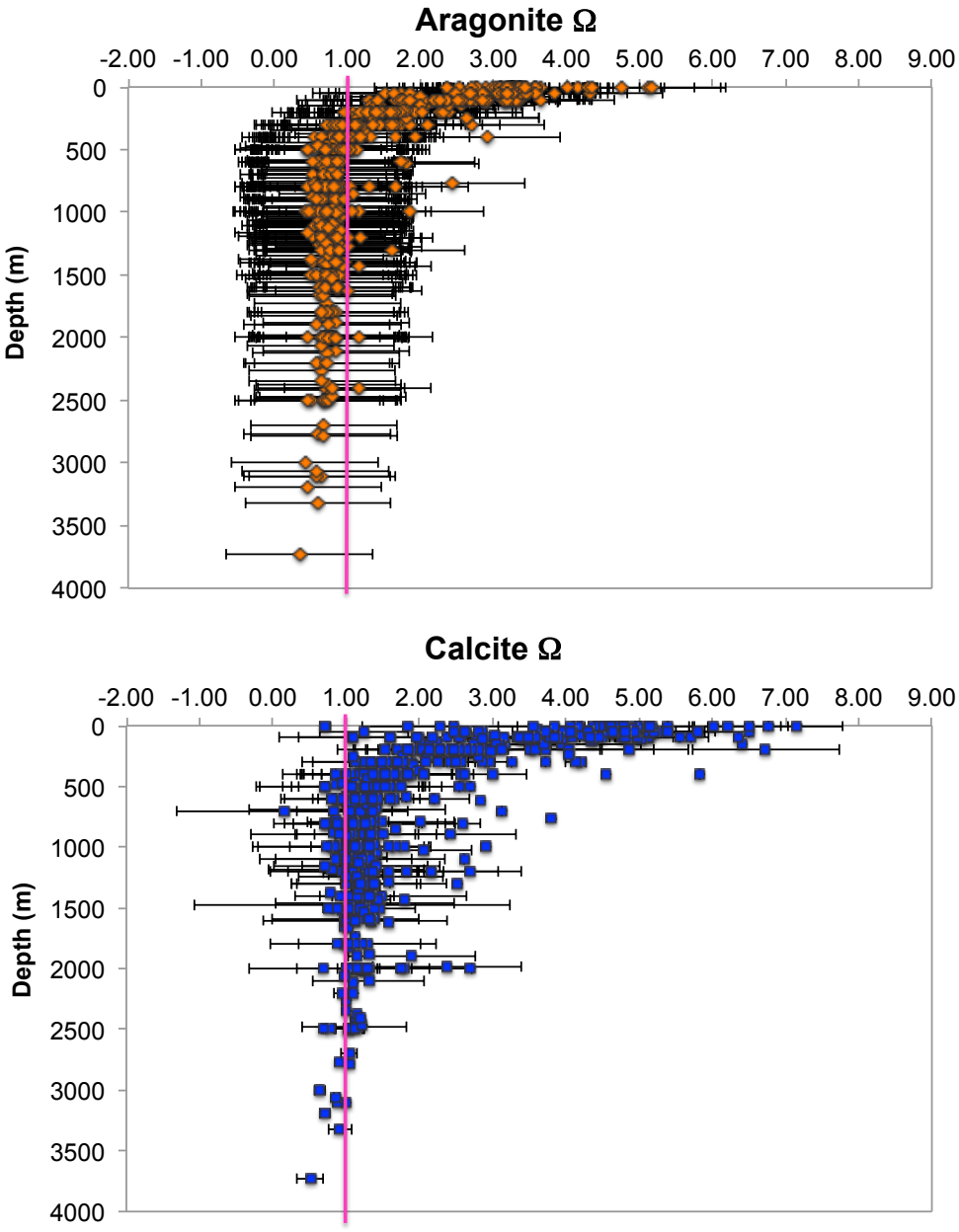

Figure 7: Compilation of calcium carbonate saturation state values including aragonite (orange diamonds) and calcite (blue squares) at all GISR stations. Ω was calculated for both aragonite and calcite using CO2sys [Pierrot, 2007]. Vertical pink line is the saturation horizon where Ω = 1 for both aragonite and calcite. The black lines show the maximum and minimum error for GISR cruises G03, G05, and G09. The saturation state error range values were calculated with CO2sys using the maximum possible DIC values along with the minimum possible TA values to find the minimum and maximum saturation state values for each bottle value.

4. DISCUSSION

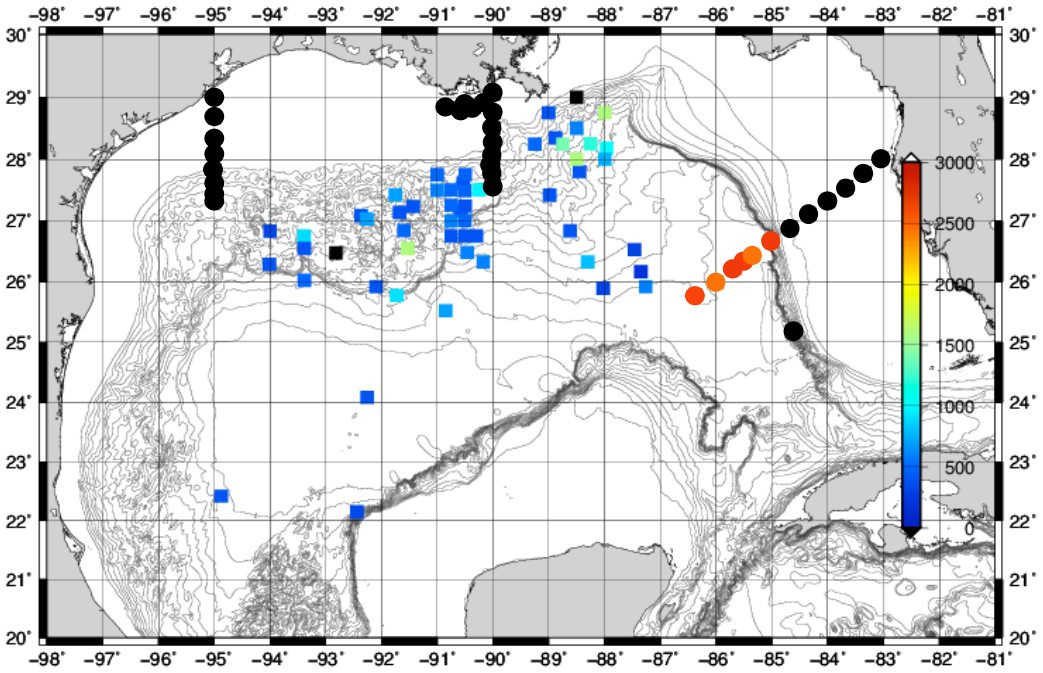

Figure 8: Aragonite saturation horizon depth (color bar) by station in the Gulf of Mexico. Squares represent the locations of GISR cruise stations while circles represent GOMECC stations. Black symbols represent stations where the AHS was not observed in the data. Data from both GOMECC cruises and all GISR cruises are included in this map.

The GOMECC1 and GOMECC2 cruises were designed to collect physical, chemical, and biological measurements to monitor the carbon system along the coast of both the northern Gulf of Mexico and the east coast of the United States. Although these cruises mainly prioritized the shelf area, the carbon data obtained for the portions of the transects on the slope were deep enough to compare these data (http://www.aoml.noaa.gov/ocd/gcc/GOMECC1/data.php and http://www.aoml.noaa.gov/ocd/gcc/GOMECC2/data.php accessed on February 25, 2016) to the GISR cruise data. GOMECC1 was completed in 2007, making results from

this cruise the only publicly available, deep water, inorganic carbon data for the GOM before the Deepwater Horizon oil spill in 2010. Researchers collected DIC and TA samples for analysis during these cruises, and these data were used to calculate pH and calcium carbonate saturation states through CO2sys. Data from both the GOMECC cruises include inorganic carbon along the shelf and a few deep stations past the shelf of western Florida (WFL), Texas (TX), and Louisiana (LA) in 2007 (GOMEEC1) and western Florida and Louisiana in 2012 (GOMECC2).

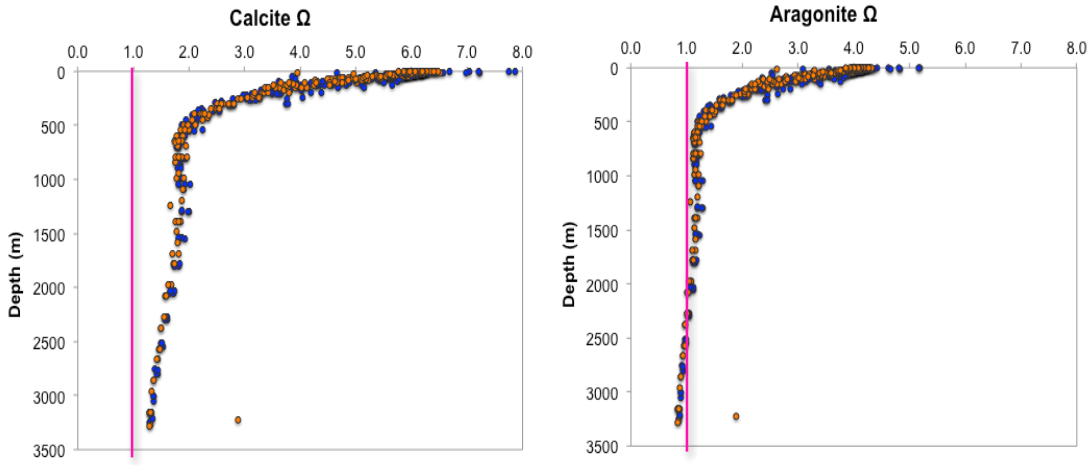

Figure 9: Calcium carbonate saturation state derived from inorganic carbon data collected during the Gulf of Mexico East Coast Carbon cruises calculated using CO2sys [Pierrot et al., 2006]. Left panel: calcite saturation state from GOMECC1 (blue circles) and GOMECC2 (orange circles). Right panel: aragonite saturation state from GOMECC1 (blue circles) and GOMECC2 (orange circles). The vertical pink line in both panels represents the saturation horizon where Ω=1.

Each station in the central GOM has an ASH around 600m (Figure 8) while the GOMECC stations in the north and central GOM did not exhibit an observed ASH. Although the WFL track covers the same area, the stations are not in the exact same location from GOMMECC1 to GOMMECC2. These stations had maximum bottle depths of 3246m for GOMECC1 and 3293m for GOMECC2. The ASH is at a depth of

approximately 2500m during GOMECC1 for both stations off the western Florida shelf and also the northern GOM (Figure 8). This depth is shallower than the ASH in the northwestern Atlantic by about 500m (Friis et al. 2007).

There is a significant upward shift in the water column of the ASH between GOMECC1 and GOMECC2 (Figure 9). There is a slight change in the calcite saturation state profile, but the saturation horizon is still not present in the water column. The ASH in GOMECC1 exists at about 2500m. Although this ASH depth is much shallower than the ASH in the northwestern Atlantic, it is relatively deep for oceans with high amounts of respiration such as the deep water masses in the Indian and Pacific oceans. During GOMECC2, the ASH is around 2300m. Because GOMECC1 and GOMECC2 are in the same track with comparable station locations and cast depths the main difference between the two is time. GOMECC1 was completed in 2007 while GOMECC2 was completed in 2012. In order for the saturation horizon depth to change this significantly over this short amount of time, there had to be a significant change in either the amount of carbon dioxide present in the water or change in alkalinity amount.

Total alkalinity in the surface of the Gulf of Mexico is usually high especially in the northwestern and central GOM due to the influx of high alkalinity freshwater from the Mississippi-Atchafalya river system (MARS). The data that show relatively constant TA profile throughout the water column at 2325umol/kg suggests entrainment of the surface water into the intermediate depth zone (Figures 4 and 5). This high alkalinity should allow for deep calcium carbonate saturation horizons because of the increase in carbonate ions from the alkalinity. However, $[CO_3^{-2}]$ was relatively low below 1000m

(Figure 6). In the northern GOM off the tip of Louisiana, the aragonite saturation horizon depth is deeper at four stations close to the MARS delta than the rest of the stations throughout the central GOM. The stations between -89° and -88°W and also above 28°N have an ASH depth around 1100m (Figures 7 and 8). The deeper horizons at these stations may be a result of the output of high alkalinity water from the Mississippi River because the influx of this freshwater signal can be observed down to around 1500m [Jochens and DiMarco, 2008]. However, the freshwater plume does travel west away from the mouth of the river, so the shallower horizons should also be observed in the northwestern GOM as well as at the GOMECC stations in the Louisiana transect. The stations in this area have saturation horizons that are closer to the average value (approximately 500m) or do not have an observed ASH (Figure 8). Figure 7 does, however, show significant error ranges for both calcite and aragonite values. As stated above, this error is the maximum error possible based on the error from DIC and TA data. Although these errors are significant, some conclusions may still be drawn from the presented data.

The GOMECC transects off the western Florida shelf on the eastern side of the GOM have saturation horizons at depths around 2250m. The loop current may be entraining some of the high alkalinity water and carrying it over to the western Florida shelf. This could be a reason why the saturation horizon in the area observed in the GOMECC data is deeper than the saturation horizon from GISR. They didn't observe any saturation horizons in the TX transect or the LA transect (Figure 8).

The GISR stations located in the central GOM have similar ASH depths to each other around the average of 600m (Figure 8). They are deeper than the northern stations of the tip of Louisiana but are consistent throughout the central GOM. This may be a result of the freshwater MARS plume that enters the GOM not affecting the intermediate waters off the coast. Because the loop current travels east instead of west, the high alkalinity water is not being entrained in the central GOM in the same way as the northern or eastern areas.

The GISR stations closer to the western boundary of the GOM have saturation horizons that are extremely shallow compared to the western Atlantic horizons and observed saturation horizons in the eastern Caribbean as well as the eastern GOM. The average depth for the AHS at the western stations is close to the average of 500m. However, the loop current is not reaching this far west in the GOM, so the surface alkalinity may not be entraining this far west. This means that the freshwater influx is not large enough to impact the intermediate water in the majority of the Gulf of Mexico. The calcite saturation horizon (CSH) was not visible in the sampled water column at any of the GISR stations (Figure 7) or the GOMECC stations (Figure 9). The profiles at each station did not have multiple consistent samples below $\Omega = 1$, so the depth of the CSH could not be determined. The aragonite saturation horizon off of west Florida shelf observed during GOMECC2 5 years later was at a depth of about 2300m (Figure 10). This is shallower than the GOMECC1 ASH by about 200m. The WFL stations from the GOMECC cruises sampled the far eastern edge of the Gulf of Mexico basin. Due to the deep water circulation in the GOM moving cyclonically, as stated by Jochens and

DiMarco [2008], the deep water on the eastern side of the GOM is younger than the water in the central and western side of the GOM. This means that there has been less time for respiration, and therefore would allow for lower amounts of inorganic carbon to be present leading to a deeper ASH on the eastern side than in the central or western side (Figures 8 and 9). The GOMECC stations that have an observable AHS exhibit much deeper saturation horizons than the data from any of the sampled GISR stations. The Texas stations from GOMECC were farther north and somewhat more west than the GISR stations, and the Louisiana stations were in a similar location as the GISR stations. Both the Texas and Louisiana stations did not have observable saturation horizons in the sampled water column for neither aragonite nor calcite. The calcite saturation horizon was not observed in the water column at any station due to solubility characteristics of calcite and also the bathymetry in the GOM. This was true for both GISR and GOMECC datasets. It is interesting to note that although the aragonite saturation horizons were very shallow, the calcite saturation horizons are not observed at all for the GISR stations. Although there is a significant influx of freshwater to the GOM with a high alkalinity signature, it is not affecting the intermediate and deep water in the majority of the GOM. This means that the inorganic carbon that is required to create shallow saturation horizons is not being buffered by a high alkalinity in the majority of the GOM. The origin of this carbon however is in question. Respiration and circulation in the Caribbean and Gulf of Mexico system are the main factors governing the available carbon in this system.

Respiration, by itself, does not seem plausible as the sole source of shoaling of a saturation horizon by 500m within a 5 to 6 year span because the apparent oxygen utilization (AOU) from the GISR cruises suggests relatively low amounts of oxygen are being consumed and converted to CO_2 through respiration (Figure 10). AOU is calculated by first calculating the amount of oxygen produced based on DIC values. The actual Winkler-measured oxygen data is subtracted from this calculated oxygen data to get the apparent oxygen utilization. AOU is reported in umol/kg. This calculation data

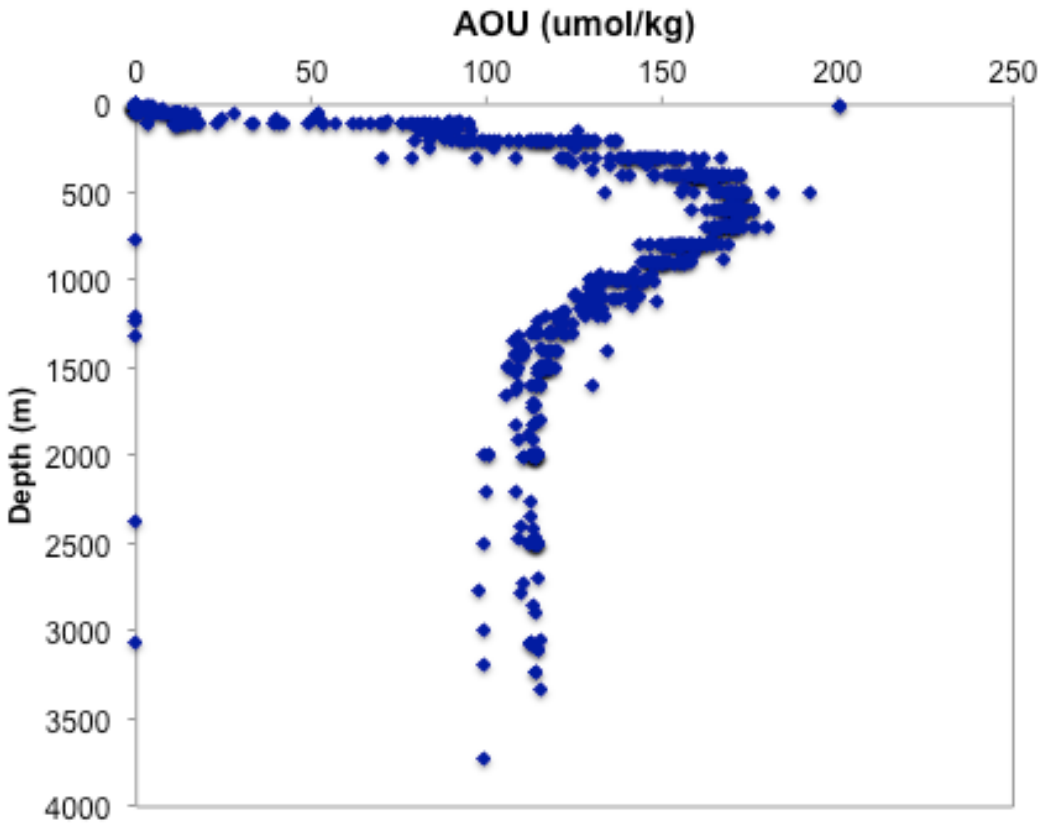

Figure 10: Compilation of calculated AOU depth profiles from GISR cruises. AOU was calculated using the Winkler dissolved oxygen data from each niskin bottle from each cast along with DIC.

was obtained for the GISR stations only (Figure 10). As depth increases, the apparent oxygen utilization is highest (170umol/kg) at about 600m mirroring the DIC data (Figure 3). This calculation describes the amount of oxygen used for respiration given the baseline oxygen for that water parcel. Because the AOU is substantial throughout the water column, respiration is a legitimate contributor to the amount of inorganic carbon present within the GOM.

It is well known that the Gulf of Mexico has a large influx of hydrocarbon from the substrate. However, the question remains whether or not this influx of hydrocarbons is the driving force of respiration in the GOM and whether or not respiration of the hydrocarbons produces enough inorganic carbon to shoal saturation horizons to 500m. Although these data were not collected as a time series, some conclusions may be drawn in terms of respiration. It is important to note that all data within the GOM was collected after the Deepwater Horizon oil (DWH) spill occurred in 2010 with the exception of GOMECC1. The hydrocarbon plume from DWH moved westward in the intermediate depth in the water column and released 3-5 million barrels of hydrocarbon into the GOM over the span of 84 days in 2010 (Camilli et al., 2010; Chanton et al. 2015; Ryerson et al., 2012; Du and Kessler, 2012). The respiration from the excess hydrocarbon may have affected the ASH depth by causing it to move shallower in the water column due to the introduction of carbon dioxide and consumption of oxygen (Du and Kessler, 2012). However, there is not enough inorganic carbon data collected in the deep GOM prior to or during the spill to verify this. The connection between respired hydrocarbon-sourced carbon and inorganic carbon within the water column is also difficult to distinguish

without isotopic signatures of the bottle samples especially without a clear source of hydrocarbons.

Most observed shoaling due to anthropogenic carbon has occurred on the order of 1-4 meters per year in the global ocean. Changes in both respiration and water mass carbon content may cause this shoaling together. As the deep water circulates around the GOM basin anticyclonically, the water could become increasingly more acidic from the increased amounts of carbon dioxide as a result of respiration. This also happens when water ages as it travels from its formation area to the north Pacific (Feely et al. 2002). The excess respiration in the GOM may be a result of the large influx of hydrocarbons from natural seeps. The GISR stations may have shallow ASHs as a result of the increased respiration within the GOM due to the hydrocarbon seeps compared to the Caribbean. Because the residence time of the deep water is relatively short and if the water entering into the GOM is relatively young, there would need to be a large amount of hydrocarbon respiration occurring either in the GOM or in the Caribbean before it gets to the GOM. However, the ASH in the WFL stations would be much shallower if there were significant amounts of respiration occurring in the Caribbean.

The shallower saturation horizon in GOMECC2 might be related to this spill due to the introduction of hydrocarbons and respiration at an increased rate. The bulk of the hydrocarbon plume did, however, move westward in the GOM, as is consistent with the known deep water circulation in the GOM, so the DWH spill probably is not able to completely account for the ASH movement in those five years [Ledwell et al. 2016; Smith et al. 2014; Mezic et al., 2010; Weisberg et al., 2016; Follett et al., 2014]. Because

shoaling of the saturation horizons are observed in both the Caribbean (A22) and in the Gulf of Mexico (GOMECC) by about 250m over a span of 5 to 6 years partnered with the suggested residence time of the Gulf of Mexico to be around 250 years, the depth of the aragonite saturation horizon is plausible in the northern central GOM around about 500m. However this study was not long enough to observe these horizons over a long amount of time and therefore it is not known how long the ASH depth observed at these stations has existed.

GOMECC2 samples were collected about a month after G01 samples, so samples from these two cruises are comparable in terms of time and season. They however have completely different saturation horizons at their respective stations especially the stations in the WFL transect compared to the central GOM. Because these samples were taken close to the same time period and have different saturation horizons, the circulation in the GOM is driving the changes between the two areas.

In order to understand the main cause of differences between the stations on the eastern side of the GOM and the central GOM, the source water to the GOM needs to also be understood. In 1997, World Ocean Carbon Experiment (WOCE) collected samples along the western Atlantic and into the eastern Caribbean (64°W and 40°N to 11°N) and called the transect A22. The World Climate Research Programme's (WCRP) Climate and Ocean: Variability, Predictability and Change (CLIVAR) repeated the transect in 2003. These data were collected to record carbon and other physical and chemical parameters in the main oceans. Data from these two cruises were used to calculate the saturation horizon in the Caribbean. Although this is only one inlet of deep water entering the

Caribbean, the deep water should have a similar signature throughout the Caribbean in both basins because the same water masses are entering into both deep passages of the Caribbean [Talley et al. 2011]. The data from 1997 show an ASH around 2000m and a calcite saturation horizon (CSH) around 4000m (Figure 11). This depth for the ASH is similar to the ASH found during the second GOMECC cruise on the eastern side of GOM and is still much shallower than the ASH on the western side of the Atlantic. Data from the repeat CLIVAR section in 2003 show an ASH around 2700m. This is a significant difference from the data collected in 1997 because there is a deepening of approximately 500-700m in approximately 6 years. This deepening is opposite to the changes observed in the GOMECC saturation horizons where there was shoaling in a similar time frame suggesting there must be some sort of chemical change in terms of inorganic carbon within that short time frame. This shift may be caused by the change in carbon dioxide content entering into the Caribbean through the source of water masses.

The Deep Western Boundary Current (DWBC) contains both Denmark Strait Overflow Water (DSOW) well below 2000m and Labrador Sea Water (LSW) at an intermediate depth between 500m and 1500m (Figure 1). Both water masses show a relatively young age signal in the cluorofluorocarbon (CFC-11) tracers and a low inorganic carbon signal because it moves relatively quickly from its formation locations down the western boundary of the north Atlantic [Talley et al., 2011]. The water masses are indistinguishable in DIC but are separated by density [Talley et al., 2011]. The general North Atlantic Deep Water mass (NADW) that fills the majority of the Atlantic basin also does not have high inorganic carbon but is much older than both water masses contained within the DWBC and is highly distinguishable from the DWBC. Because the DWBC water has two separate water masses within its current, it is likely that only the LSW has a low enough density to enter the Caribbean at the sill depths, but it is difficult to distinguish them from one another in the Caribbean if they are both entering. Increased anthropogenic carbon from deep water mass sources is probably not the sole cause of this extreme shoaling over such a short time period because in other oceans shoaling of the horizons due to anthropogenic carbon only shoal approximately 1-2m/yr, however, there is Antarctic Intermediate Water (AAIW) as well as ventilated Upper Circumpolar Deep Water (UCDW) entering the Caribbean with a high DIC signature and low CFC signature [Feely et al. 2004; Talley et al. 2011]. The evidence of UCDW entering the Caribbean in the CFC data is from the WOCE Atlantic Ocean Atlas. After travelling up the western coast of Africa, it gets upwelled and some of it is observed travelling westward across the Atlantic [Koltermann et al. 2011]. This water is observed

moving across the sill of the Jungfern passage in the A22 transect from the Atlantic into the Caribbean where its higher density causes it to fall to the bottom of the easternmost basin [Talley et al. 2011]. The CFCs in the A22 transect inside of the Caribbean show a very old CFC signal that is consistent with this ventilated UCDW in the basin. If this modified old water mass is the main source of deep water to the Caribbean and then to the GOM, then this would allow for the high CO_2 and therefore shallow ASHs in this marginal sea system. Although this sill is the main source of deepwater to the Caribbean, it is possible that Labrador Sea Water (LSW) from the DWBC is also a large source of deep water to the Caribbean if it is entering along the Windward Strait.

Another study done by S.E Georgian et. al [2015] described the inorganic carbon environment around deep water scleractinian corals on the northern shelf of the GOM. This study was also conducted after the DWH spill. They only observed undersaturation in the benthic samples at the deepest collection site around 2600m even though the lowest [CO_3^{-2}] and TA:DIC was observed at 500m. Because the group already published saturation state values and the saturation state values did not exist below 1 in the water, the carbon data from this study were not used to calculate saturation horizon depths for comparison to GISR data. This group also sampled specifically around known deep scleractinian coral locations.

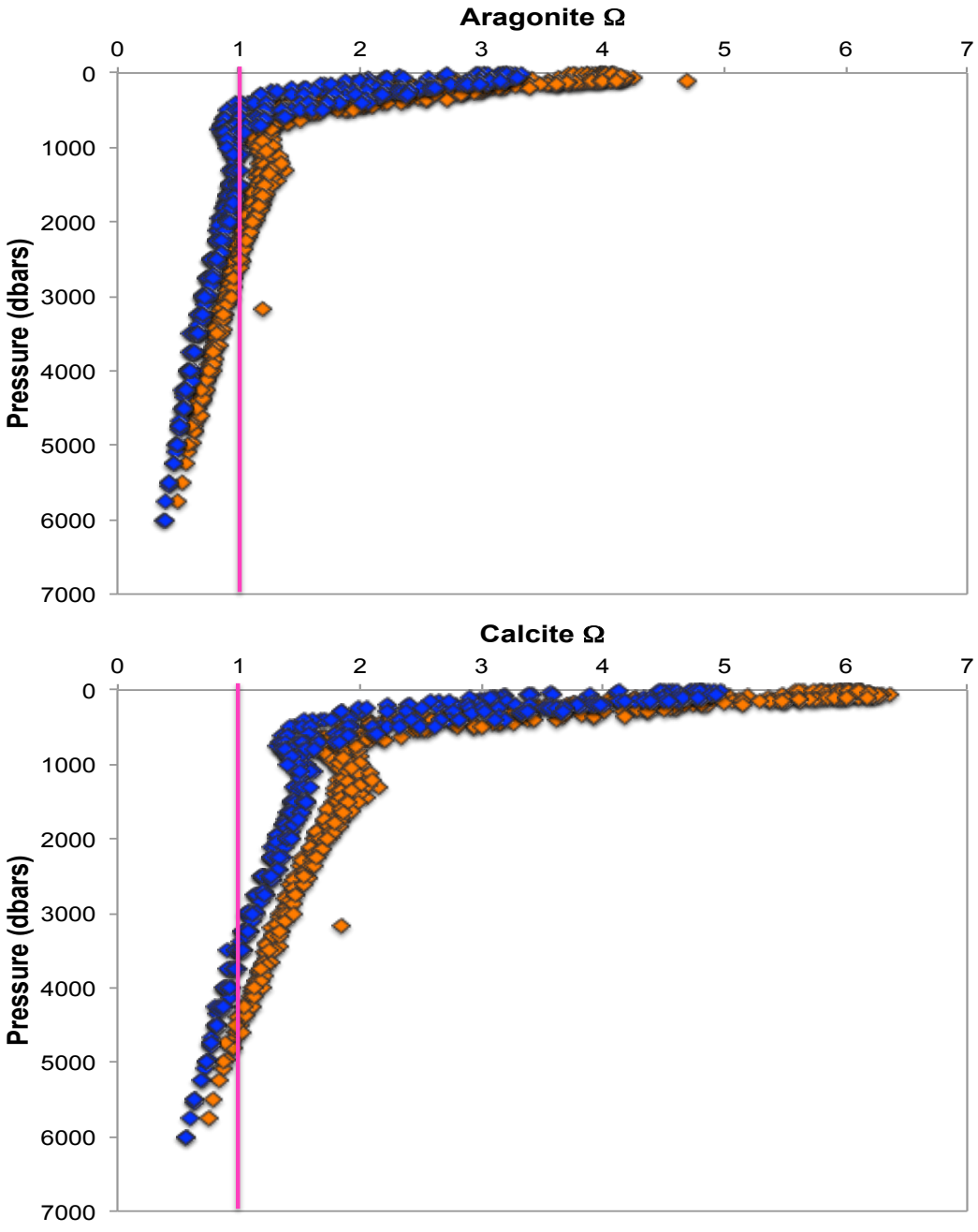

Figure 11: The calcium carbonate saturation states of WOCE transect A22 in the Caribbean (11-21.5°N, 64 °W). The top graph shows the first cruise of the aragonite saturation state from 1997 (blue) and 2003 (orange). The bottom graph shows the calcite saturation state from 1997 (blue) and 2003 (orange). The vertical pink lines represent the saturation horizon where Ω=1. Data calculated using CO2sys [Pierrot et al., 2006].

5. CONCLUSIONS

With the affects of ocean acidification becoming more and more extensive in the global ocean, monitoring calcium carbonate chemistry is increasingly important. The Gulf of Mexico has important calcifying organisms including the Flower Garden Banks National Marine Sanctuary and fisheries that rely on pH and calcium carbonate saturation of the water to be normal throughout the water column. The aragonite saturation horizon in the Gulf of Mexico gets shallower from the eastern side of the basin to the western side of the basin. This change in carbon dioxide is due most likely to large scale respiration occurring in the GOM, the cyclonic movement of deep water within the basin, and from acidic water masses entering the Caribbean from the Atlantic to form the deep water flowing from the Caribbean into the GOM. The ASH is much shallower in the GOM than in the northwestern Atlantic from which the deep water is originating. Due to significant error within the data and lack of coverage throughout the southern areas of the GOM, there needs to be further investigation of the carbon system within the GOM in order to make definite conclusions about the calcium carbonate saturation horizons.

REFERENCES

Bostock, H. C., S. E. Mikaloff Fletcher, and M. J. M. Williams (2013), Estimating carbonate paramters from hydrographic data for the intermediate and deep waters of the Southern Hemisphere oceans, *Biogeosciences*, 10, 6199-6213.

Byrne, R. H., J. G. Acker, P. R. Betzer, R. A. Feely, and M. H. Cates (1984), Water column dissolution of aragonite in the Pacific Ocean, *Nature*, 312, 321-326.

Cai, W. J. (2003), Riverine Inorganic Carbon Flux and rate of biological uptake in the Mississippi River plume. *Geophysical Res. Lett.,* 30(4), 1-4.

Chang, Y.-L. and L.-Y. Oey (2010), Eddy and Wind-Forced Heat Transports in the Gulf of Mexico, *J. of Phys. Ocean.,* 40, 2728-2742.

Carter, B. R., J. R. Toggweiler, R. M. Key, and J. L. Sarmiento (2014), Processes determining the marine alkalinity and calcium carbonate saturation state distributions, *Biogeosciences*, 22, 7349-7362.

Chanton, J., T. Zhao, B. E. Rosenheim, S. Joye, S. Bosman, C. Brunner, K. M. Yeager, A. R. Diercks, and D. Hollander (2015), using Natural Abundance Radiocarbon to Trace the Flux of Petrocarbon to the Seafloor Following the Deepwater Horizon Oil Spill, *Environ. Sci. Technol.*, 49(3), 847-854.

Chung, S.-H., K. Lee, R. A. Feely, C. L. Sabine, F. J. Millero, R. Wanninkhof, J. L. Bullister, R. M. Key, and T. –H. Peng (2003), Calcium carbonate budget in the Atlantic Ocean based on water column inorganic carbon chemistry, *Global Biogeochem. Cycles*, 17(4), 1093, doi:10.1029/2002GB002001.

Cordes, E.E., D.C Bergquist, C.R. Fisher (2009), Macro-ecology of Gulf of Mexico cold deeps, *Ann. Rev. Mar. Sci.*, 1, 143-168.

DeHaan, C. J. and W. Sturges (2005), Deep Cyclonic Circulation in the Gulf of Mexico, *J. of Phys. Ocean*. 35, 1801-1812.

Dickson, A. G., C.L. Sabine, and J.R. Christian (Eds.) 2007, Guide to Best Practices for Ocean CO_2 Measurements. PICES Special Publication 3, 191 pp.

Doney, S.C.; Fabry, V.J.; Feely, R.A.; Kleypas, J.A.; (2009), Ocean Acidification: The Other CO2 Problem, *Annual Review Marine Science* 1, 169-192.

Du, M. and J. D. Kessler (2012), Assessment of the Spatial and Temporal Variability of Bulk Hydrocarbon Respiration Following the Deepwater Horizon Oil Spill, *Environ. Sci. Technol.*, 46(19), 10499-10507.

Fantantoni, D.M., R.J. Zantopp, W. E. Johns, and J. L. Miller (1997) Updated bathymetry of the Anegada-Jungfern Passage Complex and implications for Atlantic inflow to the Abyssal Caribbean Sea, *J. Mar. Res.,*55, 847-860.

Feely, R. A., C. L. Sabine, R. H. Byrne, F. J. Millero, A. G. Dickson, R. Wanninkhof, A. Murata, Lisa. A. Miller, and D. Greeley (2012) Decadal changes in the aragonite and calcite saturation state of the Pacific Ocean, *Global Biogeochem. Cycles*, 26, GB3001, doi:10.1029/2011GB004157.

Feely, R. A., C. L. Sabine, K. Lee, W. Berelson, J. Kleypas, V. J. Fabry, F. J. Millero (2004), Impact of Anthropogenic CO_2 on the $CaCO_3$ System in the Oceans, *Science*, 3005, 362-366.

Feely, R. A., C. L. Sabine, K. Lee, F. J. Millero, M. F. Lamb, D. Greeley, J. L. Bullister, R. M Key, T. –H. Peng, A. Kozyr, T. Ono, and C.S. Wong (2002), In situ calcium carbonate dissolution in the Pacific Ocean, *Global Biogeochem. Cycles*, 16(4), 1144, doi:10.1029/2002GB001866.

Follett, L., U. Genschel, H. Hofmann (2014), A graphical exploration of the Deepwater Horizon oil spill, *Comput. Stat.*, 29, 121-132.

Friis, K., R.G. Najjar, M.J. Follows, S. Dutkiewicz, A. Körtzinger, and K.M. Johnson (2007), Dissolution of calcium carbonate: observations and model results in the subpolar North Atlantic, *Biogeosciences*, 4, 205-213.

Georgain, S. E., D. DeLeo, A. Durkin, C.E. Gomez, M. Kurman, J.J. Lunden, E.E. Cordes (2015) Oceanography patterns and carbonate chemistry in the vicinity of cold-water coral reefs in the Gulf of Mexico: Implications for resilience in a changing ocean, *Limnol. Oceanogr.*, 61, 2016, 648-665.

Gledhill, D. K., R. Wanninkhof, F. J. Millero, and M. Eakin (2008), Ocean acidification of the Greater Caribbean Region 1996-2006, *J. Geophys. Res.*, 113, C10031, doi:10.1029/2007JC004629.

Gordon, A. L. (1967), Circulation of the Caribbean Sea, *J. Geophysical Res.*, 72(24), 6207-6223.

Goyet C., R. J. Healy, and J. P. Ryan. (2000), Global distribution of total inorganic carbon and total alkalinity below the deepest winter mixed layer depths, ORNIJCDIAC-127, NDP-076. Carbon Dioxide Information Analysis Center, Oak Ridge National Laboratory, U.S. Department of Energy, Oak Ridge, Tennessee, U.S.A. 40 pp.

Guinotte, J. M., J. Orr, S. Cairns, A. Freiwald, L. Morgan, and R. George (2006, Will human-induced changes in seawater chemistry alter the distribution of deep-sea scleractinian corals?, *Ecol. Environ.,* 4(3), 141-146.

Gulf Integrated Spill Research Consortium (GISR) data obtained from https://data.gulfresearchinitiative.org/.

Gulf of Mexico and East Coast Carbon Study data obtained from http://www.aoml.noaa.gov/ocd/gcc/GOMECC1/data.php and http://www.aoml.noaa.gov/ocd/gcc/GOMECC2/data.php accessed on February 25, 2016.

Hazen, T. C., E. A. Dubinsky, T. Z. DeSantis, G. L. Andersen, Yvette M. Piceno, N. Singh, J. K. Jansson, A. Probst, S. E. Borglin, J. L. Fortney, W. T. Stringfellow, M. Bill, M. E. Conrad, L. M. Tom, K. L. Chavarria, T. R. Alusi, R. Lamendella, D. C. Joyner, C. Spier, J. Baelum, M. Auer, M. L. Zemla, R. Chakraborty, E. L. Sonnenthal, P. D'haelseleer, H-Y N. Holman, S. Osman, Z. Lu, J. D Van Nostrand, Y. Deng. J. Zhou, and O. U. Mason (2010), Deep-Sea Oil Plume Enriches Indigenous Oil-Degrading Bacteria, *Science*, 330, 204-208, doi:10.1126/science.1195979

Honjo, S. and J. Erez (1978) Dissolution rates of calcium carbonate in the deep ocean; an in-situ experiment in the north Atlantic ocean, Earth and Plantery Science Letters, 40, 287-300.

Jochens, A. E. and S. F. DiMarco, (2008). Physical Oceanraphic condiions in he deepwaer Gulf of Mexico in summer 2000-2002. *Deep-Sea Res. II.* 55, 2541-2554.

Joyce, T. M., R. S. Pickart, and R. C. Millard (1999) Long-term hydrographic changes at 52 and 66°W in the north Atlantic Subtropical Gyre & Caribbean, *Deep-Sea Res. II,* 46, 245-278.

Joye, S.B., A. Bracco, T.M. Özgökmen, J.P. Chanton, M. Grosell, I.R. MacDonald, E.E. Cordes, J.P. Montoya, and U. Passow (2016) The Gulf of Mexico ecosystem, six years after the Macondo oil well blowout, *Deep-Sea Res. II,* 129, 4-19.

Keul, N., J.W. Morse, R. Wanninkhof, D.K. Gledhill, and T.S. Bianchi (2010), Carbonate chemistry dynamics of surface waters in the northern Gulf of Mexico. *Aquatic Geochemistry* 16:337-351.

Koltermann, K.P., V.V. Gouretski, and K. Jancke (2011) Hydrographic Atlas of the World Ocean Circulation Experiment (WOCE). Volume 3: Atlantic Ocean (eds. M. Sparrow, P. Chapman and J. Gould). International WOCE Project Office, Southampton, UK, ISBN 090417557X.

Ledwell, J.R., R. He, Z. Xue, S.F. DiMarco, L. Spener, and P. Chapman (2016) Dispersion of a tracer in the deep Gulf of Mexico. *J. of Geophys. Res.,* 121, 1110-1132, doi: 10.1002/2015JC011405.

Lunden, J.J., S.E. Georgian, and E.E. Cordes (2013), Aragonite saturation states at cold-water reefs structured by *Lophelia pertusa* in the Northern Gulf of Mexico. *Limnology and Oceanography,* 58:354-362.

MacDonald, I. R., N.L. Guinasso Jr., S.G. Ackleson, J. F. Amos, R. Duckworth, R. Sassen, and J.M. Brooks (1993), Natural oil slicks in the Gulf of Mexico visible from space, *J. Geophys. Res.*, 98 (C9), 16351-16364.

MacDonald, I.R., M. Kastner, and I. Leifer (2005) Estimates of natural hydrocarbon flux in the Gulf of Mexico basin from remote sensing data, *Geophys, Res. Abstracts: EGU,* 7, 09970.

Mansour, A.S. (2014), Hydrocarbon-derived carbonates along the upper-lower continental slope, Gulf of Mexico: a mineralogical and stable isotopic study, *Carbonate Evaporites,* 29, 89-105.

Maul, G.A. and F. M. Vukovich (1993), The Relationship between Variations in the Gulf of Mexico Loop Current and Straits of Florida Volume Transport. *J. of Phys. Ocean.*, 23, 785-796.

Mendoza, V.M., E. E. Villanueva, and Adem, J. (2005) On the annual cycle of sea surface temperature and mixed layer depth in the Gulf of Mexico. *Atmospherá.* 127-141.

Mezic, I., S. Loire, V. A. Fonoberov, and P. Hogan (2010), A new mixing diagnostic and Gulf oil spill movement, *Sci.,* 330, 486-489.

Millero, F. J. (2007), The Marine Inorganic Carbon Cycle, *Chem. Rev.,* 107, 308-341.

Nipper, M., Sánchez Chávez, J.A., and Tunnell, J.W., Jr. (eds), 2008. Gulfbase: Resource Database for Gulf of Mexico Research. World Wide Web electronic publication. Available from: http://www.gulfbase.org.

Osborne, A. H., B. A Haley, E. C Hathorne, S. Flögel, and M. Frank (2014), Neodymium isotopes and concentrations in Caribbean seawater: Tracing water mass mixing and continental input in a semi-enclosed ocean basin, *Earth and Planetary Sci. Lett.,* 406, 174-186.

Patsavas, M. C., R. H. Byrne, B. Yang, R. A. Easley, R. Wanninkhof, and X. Liu (2015) Procedures for direct sspectrophotometric determination of carbonate ion concentrations: Measurements in US Gulf of Mexico and East Coast waters, *Mar. Chem.*, 168, 80-85.

Paulmier, A., D. Ruiz-Pino, and V. Garçon (2011), CO_2 maximum in the oxygen minium zone (OMZ), *Biogeosci.*, 8, 239-252, doi:10.5194/bg-239-2011.

Pierrot, Lewis, D. E., Wallace, D. W. R. (2006) MS Excel Program Developed for CO2 System Calculations. ORNL/CDIAC-105a. Carbon Dioxide Information Analysis Center, Oak Ridge National Laboratory, U.S. Department of Energy, Oak Ridge, Tennessee. doi: 10.3334/CDIAC/otg.CO2SYS_XLS_CDIAC105a.

Pohlman, J. W., J. E. Bauer, W. F. Waite, C. L. Osburn, and N. R. Chapman (2010), Methane hydrate-bearing seeps as a source of aged dissolved organic carbon to the oceans, *Nature Geoscience,* 4, 37-41, doi:10.1038/NGE01016.

Raymond, P.A. and Cole, J.J. (2003) Increase in the Export of Alkalinity from North America's Largest River, *Science,* 301:88-90.

Rivas, D., A. Badan, and J. Ochoa (2005) The Ventilation of the Deep Gulf of Mexico. *J. of Phys. Ocean.,* 35: 1763-1781.

Ryerson, T. B., R. Camilli, J. D. Kessler, E. B Kujawinski, C. M. Reddy, D. L. Valentine, E. Atlas, D. R. Blake, J. de Gouw, S. Meinardi, D. D. Parrish, J. Peischl, J. S Seewald, and Carsten Warneke (2012), Chemical data quantify *Deepwater Horizon* hydrocarbon flow rate and environmental distribution, *PNAS*, 109(50), 20246-20253.

Sabine, C. L., R. A. Feely, N. Gruber, R. M. Key, K. Lee, J. L. Bullister, R. Wanninkhog, C.S. Wong, D. W. R. Wallace, B. Tilbrook, F. J. Millero, T.-H. Peng, A.

Kozyr, T. Ono, and A. Rios (2004) The Oceanic Sink for Anthropogenic CO_2: Past, Present, and Future, *Science*, 305 (5682), 367-371.

Sarma, B. B., S. S. T. Ono, and T. Saino (2002), Increase of total alkalinity due to shoaling of aragonite saturation horizon in the Pacific and Indian Oceans: influence of anthropogenic carbon inputs, *Geophys. Res. Lett.,* 29(20), 1971, doi:10.1029/2002GL015135.

Schwartz, J. and R. Rendle-Bühring (2005) Controls on modern carbonate preservation in the southern Florida Straits, *Sed. Geol.,* 175, 153-167.

Sheng, J. and L. Tang (2003), A numerical study of circulation in the western Caribbean Sea, *J. of Phys. Ocean.,* 33, 2049-2069.

Smith, R.H., E.M. Johns, G.J. Goni, J. Trinanes, R. Lumpkin, A.M. Wood, C.R. Kelble, S.R. Cummings, J.T. Lamkin, and S. Privoznik (2014), Oceanographic conditions in the Fulf of Mexico in July 2010 during the Deepwater Horizon oil spill, *Continental Shelf Res,* 77, 118-131.

Solomon, E.A., M. Kastner, I.R. MacDonald, and I. Leifer (2009) Considerable methane fluxes to the atmosphere from hydrocarbon seeps in the Gulf of Mexico, *Nat. Geosci.*, 2, 564-565.

Stalcup, M.C., W.G. Metcalf, and R. G. Johnson (1975) Deep Caribbean inflow through the Anegad-Jungfern passage, *J. Mar. Res.*, 33, 15-35.

Sturges, W. (1970) Observations of Deep-Water Renewal in the Caribbean Sea, *J. of Geophys. Res.,* 75:7602-7610.

Sverdrup, H. U., M. W. Johhnson, and R. H. Fleming (1942) *The Oceans, Their Physics, Chemistry, and General Biology.* New York, New York.

Talley, L. D., G. L. Pickard, W. J. Emery, J. H. Swift (2011), Descriptive Physical Oceanography An Introduction, Elsevier Inc., Oxford, UK.

Thunell, R. C. (1982) Carbonate Dissolution and Abyssal Hydrography in the Atlantic Ocean, *Mar. Geology*, 47, 165-180.

Wang, Z. A., R. Wanninkhof, W.-J. Cai, R. H. Byrne, X. Hu, T.-H. Peng, and W.-J. Huang (2013), The marine inorganic carbon system along the Gulf of Mexico and Atlantic coasts of the United States: Insights from a transregional coastal carbon study, *Limnol. Oceanogr.*, 58(1), 325-342.

Weisberg, R. H., L. Zheng, Y. Liu, and S. Murawski (2016), Did Deepwater Horizon hydrocarbons transit to the west Florida continental shelf?, *Deep-sea Res. II*, 129, 259-272.